Materials Today Physics 5 (2018) 72–77

Contents lists available at ScienceDirect

Materials Today Physics

journal homepage: https://www.journals.elsevier.com/materials-today-physics

Electronic band structure of carbon honeycombs

Zhenqian Pang [a, b], Xiaokun Gu [c], Yujie Wei [a, b, **], Ronggui Yang [d, e, *]

[a] LNM, Institute of Mechanics, Chinese Academy of Sciences, Beijing, People's Republic of China
[b] School of Engineering Sciences, University of Chinese Academy of Sciences, Beijing, China
[c] Institute of Engineering Thermophysics, Shanghai Jiao Tong University, Shanghai, China
[d] Materials Science and Engineering Program, University of Colorado, Boulder, Colorado, USA
[e] Department of Mechanical Engineering, University of Colorado, Boulder, Colorado, USA

ARTICLE INFO

Article history:
Received 17 May 2018
Received in revised form
26 June 2018
Accepted 26 June 2018

Keywords:
Ultralight weight
sp^3 hybridization
Semiconductor
Band gap
Boron-honeycomb
Phonon dispersion

ABSTRACT

In this article, we present the electronic properties of various carbon honeycombs (C-honeycombs) with different cell sizes and junction types based on *ab initio* calculations. Among the three typical C-honeycombs with junctions connected via the zigzag edge, the armchair edge, or the hybrid edges of graphene nanoribbons, it is found that the zigzag C-honeycombs and the hybrid ones exhibit metallic properties. However, the armchair C-honeycombs are metallic only if the number of atomic planes N of the graphene nanoribbon in the C-honeycomb sidewall follows $N = 3p+1$, with p as an integer and are semiconducting for other N. For those semiconducting ones, the bandgap of the C-honeycomb is about 1.19 eV with the narrowest sidewall (5.2 Å) and monotonically decreases to about 0.15 eV when the width is increased to 34.8 Å. The semiconducting nature of such C-honeycombs with nanometer size pores may be used for lightweight semiconductor in electronic devices or supercapacitor energy storage. As a comparison, we show that all boron honeycombs are metallic, and their electronic properties are independent of sidewall widths.

Graphene has extremely high strength [1], high electrical and thermal conductivity [2,3], and many other appealing physical and chemical properties [4]. Owing to its nature with zero bandgap [5], different strategies have been proposed to open the electronic bandgap of pristine graphene. For example, the substrate-induced bandgap opening method [6,7] and tensile straining [8] may lead to a small bandgap in pristine graphene. By cutting large-area graphene into nanoribbons, distinct electronic properties were observed in contrast to the pristine graphene sheets. Further studies indicate that both the edge-type and ribbon width may affect the electronic properties of graphene nanoribbons (GNRs) [9–17]. The bandgap is a primary effect of large number of defects in such GNRs. Indeed, grain boundaries in polycrystalline graphene could also introduce a small bandgap per the first principle calculations [9–17]. With the success of carbon honeycomb (C-honeycomb) synthesis [18] and the identification of stable three-dimensional (3-D) structures [19,20], it would be of interest to examine the electronic properties of those stable 3-D C-honeycombs constructed by graphene sheets of different chirality since they inherit both the GNR structures and the grain boundary defects. In this article, we show how the sidewall width and junction type may influence the electronic properties of C-honeycombs. Borophene is another two-dimensional material, which might form honeycomb structures as well. Here, we also study the electronic properties of boron-honeycombs (B-honeycombs) and compare them with C-honeycombs.

As detailed in the study by Pang et al [19], a C-honeycomb is composed of GNRs by forming junctions with hybrid sp^2 and sp^3 bonding. Stable zigzag GNRs form 5-5-8 junction of C-honeycomb (ZZ-CH), while the armchair GNRs form 6-6-6 junction of C-honeycomb (AC-CH). A hybrid C-honeycomb structure, with alternative 5-5-8 junction and 6-6-6 junction can also be formed. Two types of combination, with sp^2 bonding in the sidewall and sp^3 bonding in the junction exist not only in the zigzag and armchair C-honeycomb structures but also in the hybrid structures. To analyze how the bonding hybridization may influence the electronic properties, we denote the junction atoms (in red color) as C1 and the sidewall atoms (in blue color) as C2, as shown in Fig. 1a.

* Corresponding author. Materials Science and Engineering Program, University of Colorado, Boulder, Colorado, 80309, USA.
** Corresponding author. LNM, Institute of Mechanics, Chinese Academy of Sciences, Beijing, 100190, People's Republic of China.
E-mail addresses: yujie_wei@lnm.imech.ac.cn (Y. Wei), ronggui.yang@colorado.edu (R. Yang).

https://doi.org/10.1016/j.mtphys.2018.06.003
2542-5293/

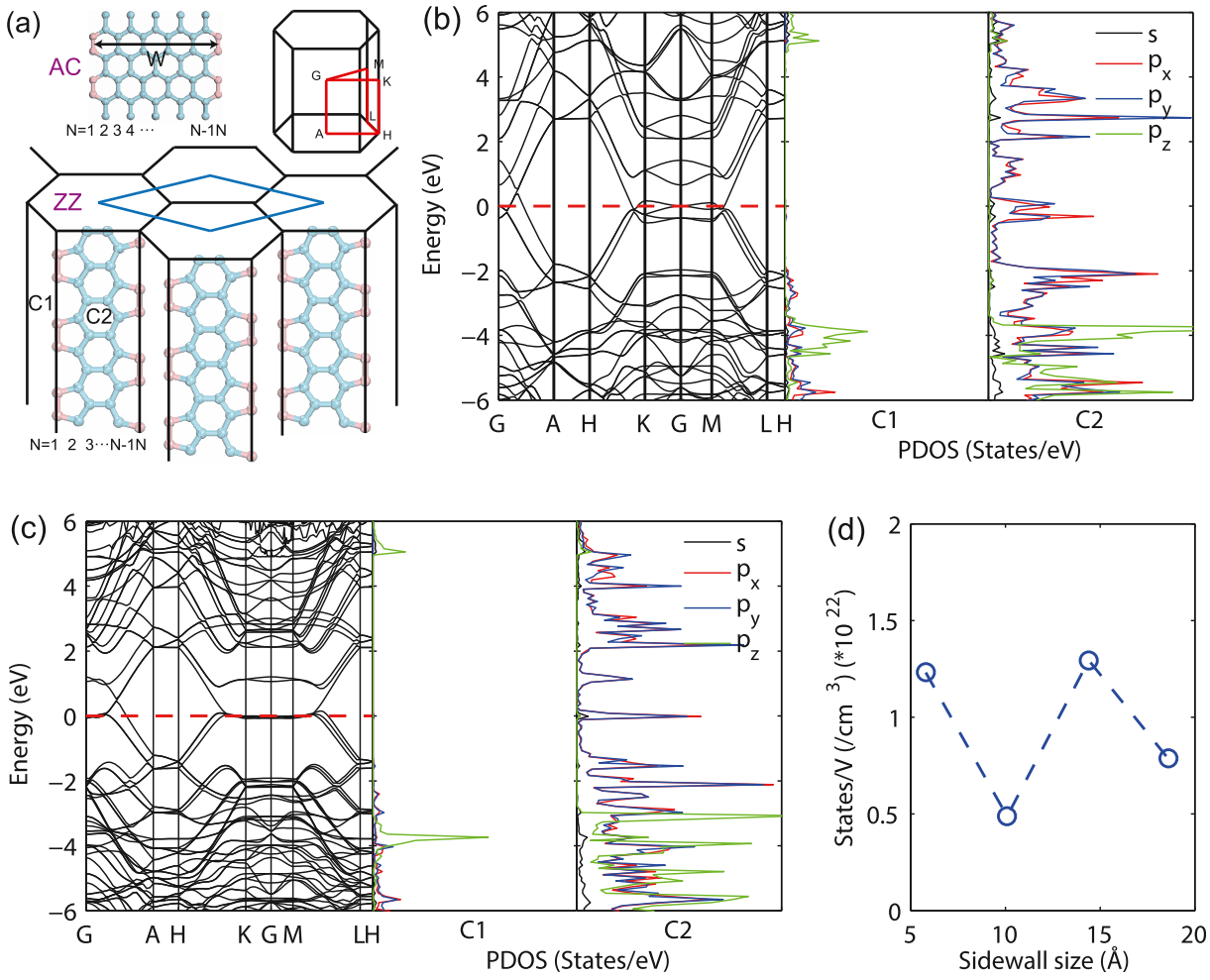

Fig. 1. Electronic band structure of zigzag C-honeycombs of different sizes. (a) Atomistic structure of sidewall in ZZ-CH and AC-CH. The inset at the top-right corner is the first Brillouin zone used to present the electronic band structures. Electronic band structures ($E-E_F$) and projected density of states of different kinds of atoms in the zigzag C-honeycombs with different sidewall widths: (b) 5.8 Å; (c) 10.1 Å. (d) States of the Fermi level average in the volume as a function of sidewall size. PDOS, projected density of states.

As illustrated in Fig. 1a, the size of C-honeycombs is identified by the width of the sidewall which is a GNR. The width W of a GNR is obtained as

$$W = \frac{(N-1)\sqrt{3}}{2}a_0 \tag{1}$$

for GNRs with armchair edges along the ribbon direction (armchair GNRs), and

$$W = \left(\left[\frac{N}{2}\right] + \frac{1}{2}\left[\frac{N-1}{2}\right]\right)a_0 \tag{2}$$

for GNRs with zigzag edges along the ribbon direction (zigzag GNRs), where N is the number of atomic planes of the graphene ribbon, and a_0 is the length of C-C bonds. The bracket [x] in Eq. (2) represents the integer function, which means the largest integer smaller than x.

We use the Vienna *ab* initio simulation package [21,22] to calculate the electronic band structures. Calculations are based on the projector augmented wave pseudopotentials [23] and the generalized gradient approximation of the Perdew–Burke–Ernzerhof functional [24]. The kinetic energy cut-offs for the plane-wave basis set are 520 eV for C-honeycomb and 400 eV for B-honeycomb. A 3×3×6 Monkhorst–Pack k-mesh is used for the reciprocal space of a primitive unit cell of ZZ-CH and AC-CH (width $W < 20$Å others, the atomic force convergence bar is set as $1e^{-2}$ eV/Å). The stability calculation of the hybrid C-honeycombs is completed by phonon dispersion analysis using the supercell method by Phonopy package [25]. The system is relaxed by setting the atomic force to be $1e^{-5}$ eV/Å to satisfy the required accuracy in phonon dispersion calculations.

We show in Fig. 1, the electronic band structures of ZZ-CHs of different sidewall widths. It is rather obvious that ZZ-CHs are metallic. To understand the origin of these electronic properties, we calculated the projected density of states of two types of carbon atoms (C1 and C2). As shown in Fig. 1b and Fig. 1c, there is negligible contribution from C1 atoms to the density of states (DOSs) around the Fermi level. Major contribution comes from the $2p_x$ and $2p_y$ orbitals in C2 atoms. These two projected DOS contribute equally to the metallic property. The band structures of the ZZ-CH with the sidewall width 10.1 Å (Fig. 1c) resemble those in GNRs [16,17] but differ greatly from that of the zigzag nanotubes [26]. These electronic band structures indicate that there will be a peak at the Fermi level for ZZ-CHs. The electrical conductivity is mainly dominated by the DOS $3k_BT$ close to the Fermi level, where k_B is the Boltzmann constant and T is the temperature in Kelvin. Fig. 1d shows the average electronic density (per atom) in those C-honeycombs. Although carrier concentration does not change

monotonically with the increased width, they are in the same order of magnitude with those of most metals [27].

The electronic band structures of armchair AC-CH of different sizes are shown in (Fig. 2). These structures exhibit both semiconducting and metallic properties, which are distinct from those of the ZZ-CH ones. When $N = 3p+1$ (where p is a positive integer), the AC-CH structure is metallic, while AC-CHs are semiconducting when $N = 3p$ and $N = 3p+2$. It is worth noting that these electronic band structures are different from those of armchair GNRs [13] calculated by tight-binding model and the first-principles method, in which the GNRs show semiconducting properties if $N=3p+1$. From the DOS of semiconducting AC-CHs, the first peak below the Fermi level is close to the valence band when $N=3p+2$; if $N=3p$, the peaks are typically far away from the top of valence band. With the increasing sidewall width, the first peak in the valence band moves to the top of valence band.

We also calculated the contribution of each orbital to the metallic structures (Fig. 2c). Similar to those in ZZ-CHs, $2p_x$ and $2p_y$ orbitals of C2 atoms dominate the electronic DOS around the Fermi level, and the two orbitals have equal contributions; the contribution from the C1 atoms is also negligible. Recently, a new stable metallic carbon allotrope (Hex-C_{18}) was predicted [28], and the dominant contribution to metallic nature of this novel structure was found to come from $2p_z$ orbitals of C2 atoms.

The width-dependent electronic properties of AC-CH can be explained by adopting the energy band analysis for zigzag nanotubes where their electronic states near the Fermi level are originated from π. The energy dispersion relation $E_m(k)$ of the zigzag nanotubes of width N is given as [29]:

$$E_m(k) = \pm\gamma_0\left\{1\pm 4\cos\frac{\sqrt{3}ka}{2}\cos\frac{m\pi}{N-1}+4\cos^2\left(\frac{m\pi}{N-1}\right)\right\}^{1/2}\left(-\frac{\pi}{\sqrt{3}}<ka<\frac{\pi}{\sqrt{3}}\right)\left(m=1,\ldots,\frac{N-1}{2}\right) \quad (3)$$

where γ_0 is the nearest-neighbor transfer integral and $a = \sqrt{3}a_0$, and k is a one-dimensional vector along the axial direction. Since the atomic structure of the GNRs in the AC-CHs is similar to that of the zigzag nanotubes and the edges of the nanoribbons only occupy a small fraction, the nanoribbons are thus expected to largely retain the electronic properties of zigzag nanotubes. Therefore, the size dependent band structure of AC-CHs could be explained by Eq. (3) for zigzag carbon nanotubes [29–31].

We present the electronic bandgaps of semiconducting AC-CHs as a function of the sidewall width in Fig. 3. In AC-CHs, the electronic bandgap decreases with the increasing sidewall width. This

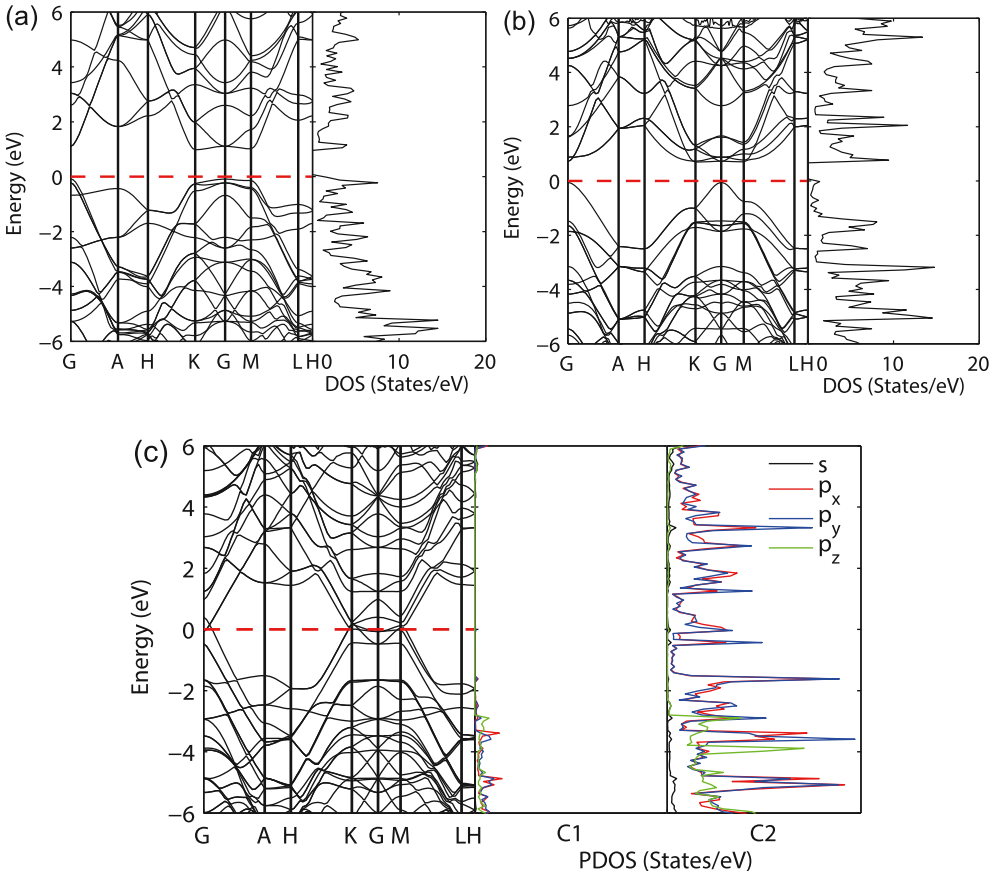

Fig. 2. Electronic band structure ($E-E_F$) and total density of states of armchair C-honeycombs with different sidewall widths: (a) W = 5.2 Å (N = 5); (b) W = 6.5 Å (N = 6). (c) Electronic band structure ($E-E_F$) and projected density of states of carbon honeycomb with sidewall width W = 7.7 Å (N = 7). DOS, density of state; PDOS, projected density of states.

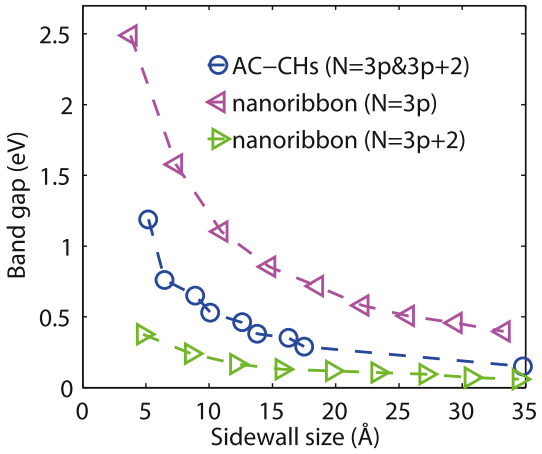

Fig. 3. Comparison of electronic bandgaps of AC-CHs with different sidewall width. The results of carbon nanoribbons calculated using local density approximation pseudopotential are also plotted for comparison [13].

means that the width of graphene ribbons determines the changing trend of electronic bandgaps in the AC-CHs. When the sidewall width is increased to W = 34.8 Å, the electronic bandgap is decreased to about 0.15 eV, which is still greater than zero.

We further calculate the electronic properties of the hybrid system with 5-8-6 rings (Fig. 4). In such C-honeycomb, the junction is also composed of sp^3 hybridized bonding, with one-side similar to the ZZ-CHs and the other side resembling that in the AC-CHs. Here, we calculate first the phonon dispersion of the smallest hybrid honeycomb and find that all phonon frequencies are positive, which indicates that these structures are mechanically and thermodynamically stable. Note that the two sidewalls are at different widths with a=4.4 Å, b=5.8 Å (Fig. 4b). The electronic properties of the structures with different sidewall widths are shown in Fig. 4c. These structures show that the hybrid honeycombs are metallic. The introduction of the hybrid junction, one as that in the ZZ-CH and the other in AC-CH cannot open the bandgap. From Fig. 4c, we see that the dominant metallic feature comes from the $2p_y$ orbital. Compared with the electronic DOS of the ZZ-CH and the AC-CH ones, the projected DOS of hybrid C-honeycomb in $2p_x$

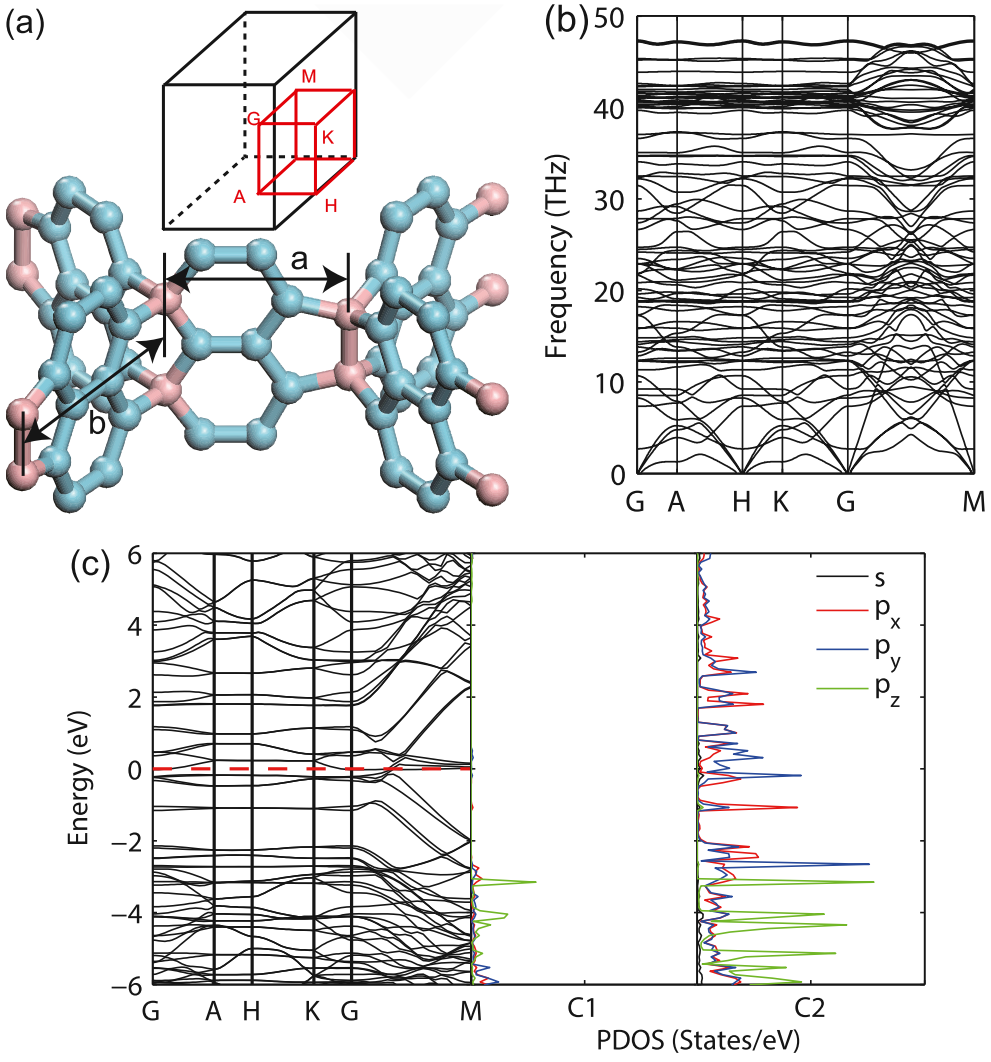

Fig. 4. (a) Local atomistic structure of 5-8-6 hybrid system and the first Brillouin zone of structure used to calculate the band structures. Here the junction atoms are denoted as C1 (red) while the sidewall atoms are denoted as C2 (blue), same as the previous definition. (b) Phonon dispersion of the hybrid structure with the sidewall size: a = 4.4 Å, b = 5.8 Å. (c) The band structures (E-E_F) and projected density of states of hybrid structures. PDOS, projected density of states. (For interpretation of the references to color in this figure legend, the reader is referred to the Web version of this article.)

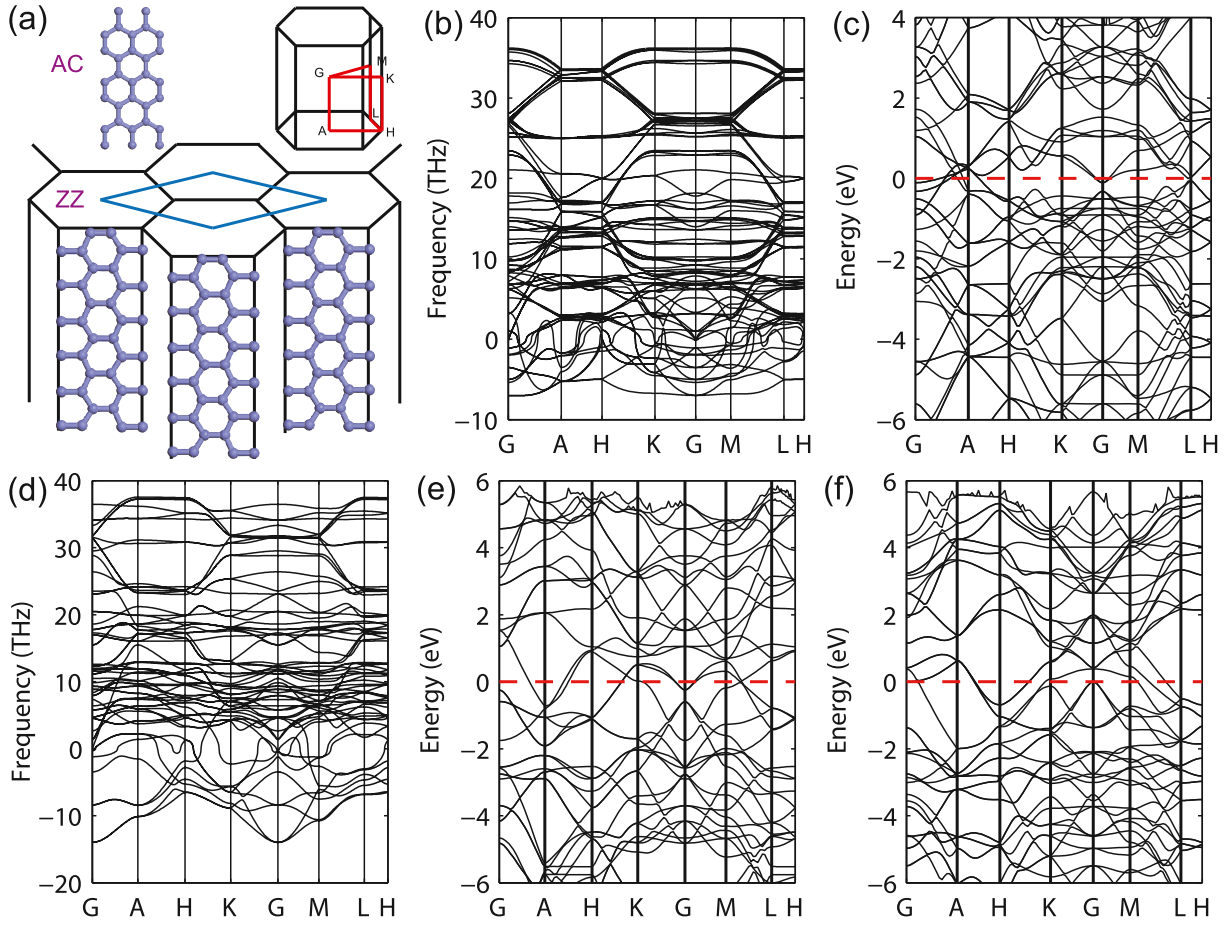

Fig. 5. Phonon dispersion and electronic band structure of B-honeycombs with different junctions. (a) Atomistic structure of sidewall in ZZ-BH and AC-BH. The inset at the top-right corner is the first Brillouin zone used for the phonon dispersion and electronic band structures calculations. (b)Phonon dispersion and (c) electronic band structures of ZZ-BH with the sidewall width: 6.2 Å. (d) Phonon dispersion of AC-BH with the sidewall width: 4.4 Å. Electronic band structures of AC-BHs with the different sidewall widths: (e) 4.4 Å (N = 5), (f) 5.4 Å (N = 6).

and $2p_y$ orbitals is significantly different, owing to the structural difference in the junction.

We present a comparison of electronic band structure of C-honeycomb with B-honeycomb, and the latter seems to be stable as well when deposited on a substrate [32]. We consider the same type of junctions in B-honeycomb as in C-honeycomb, and term B-honeycombs as ZZ-BH and AC-BH, if borophene ribbons are connected along the zigzag edge and the armchair edge for the three-dimensional structure, respectively. In comparison with C-honeycombs, B-honeycombs with zigzag nanoribbons collapse when sp^3 bonding is considered in the junctions. The relaxed atoms in the junction in ZZ-BH are sp^2 hybrid bonding, as shown in Fig. 5a. We also calculate the phonon dispersion of the smallest zigzag B-honeycomb to examine the stability of ZZ-BH (Fig. 5b). Negative frequencies are observed in the phonon dispersion. From the stability analysis of free-standing borophene [32], we conclude that ZZ-BH may need suitable substrates to maintain its structural stability. Fig. 5c shows the band structures of ZZ-BHs. Here, all these structures exhibit metallic properties. From the phonon dispersions and electronic band structures of AC-BHs, as shown in Fig. 5d–f, negative phonon frequencies are seen (Fig. 5d). By defining the number of atomic planes (N) of the borophene ribbon as the same with C-honeycomb, we see B-honeycombs of different sidewall widths are metallic.

In conclusion, we calculate the electronic band structures of several mechanically stable 3-D C-honeycombs, which is mechanical stable and is of signficance for the scale-up of 3-D graphene [18–20,33]. We reveal that both ZZ-CHs and the hybrid ZZ and AC honeycombs are metallic, while AC-CH ones may be either metallic or semiconducting: It is metallic only if $N = 3p+1$, but it is semiconducting when $N = 3p$ and $N=3p+2$. For the latter case, the bandgap of these semiconducting AC-CHs decreases with the increase of the sidewall width. The bandgap is as low as 0.15 eV in the AC-CHs when the sidewall width is increased to 34.8 Å. The metallic nature of ZZ-CH and AC-CHs originates from the equal contribution from the $2p_x$ and $2p_y$ orbitals. In contrast, the two orbitals exhibit distinct contribution in the hybrid C-honeycomb. All these B-honeycombs structures studied here are instable without the support of suitable substrates, and they exhibit metallic nature.

Acknowledgments

Y.W. acknowledges the support from National Natural Science Foundation of China (NSFC) (11425211). The calculations are performed at the Supercomputing Center of CAS.

References

[1] C. Lee, et al., Measurement of the elastic properties and intrinsic strength of monolayer graphene, Science 321 (5887) (2008) 385–388.

[2] S. Ghosh, et al., Extremely high thermal conductivity of graphene: Prospects for thermal management applications in nanoelectronic circuits, Appl. Phys. Lett. 92 (15) (2008) 151911.
[3] J.H. Seol, et al., Two-dimensional phonon transport in supported graphene, Science 328 (5975) (2010) 213–216.
[4] Z. Zhang, C. Chen, W. Guo, Magnetoelectric effect in graphene nanoribbons on substrates via electric Bias Control of Exchange Splitting, Phys. Rev. Lett. 103 (18) (2009) 187204.
[5] A.C. Neto, et al., The electronic properties of graphene, Rev. Modern Phys. 81 (1) (2009) 109.
[6] G. Giovannetti, et al., Substrate-induced band gap in graphene on hexagonal boron nitride: ab initio density functional calculations, Phys. Rev. B 76 (7) (2007) 073103.
[7] S.Y. Zhou, et al., Substrate-induced bandgap opening in epitaxial graphene, Nat. Mater. 6 (10) (2007) 770–775.
[8] F. Guinea, M. Katsnelson, A. Geim, Energy gaps and a zero-field quantum Hall effect in graphene by strain engineering, Nat. Phys. 6 (1) (2010) 30–33.
[9] L. Brey, H.A. Fertig, Electronic states of graphene nanoribbons studied with the Dirac equation, Phys. Rev. B 73 (23) (2006) 235411.
[10] Z. Chen, et al., Graphene nano-ribbon electronics, Phys. E Low-dimens. Syst. Nanostruct. 40 (2) (2007) 228–232.
[11] M.Y. Han, et al., Energy band-gap engineering of graphene nanoribbons, Phys. Rev. Lett. 98 (20) (2007) 206805.
[12] K. Nakada, et al., Edge state in graphene ribbons: nanometer size effect and edge shape dependence, Phys. Rev. B 54 (24) (1996) 17954–17961.
[13] Y.-W. Son, M.L. Cohen, S.G. Louie, Energy gaps in graphene nanoribbons, Phys. Rev. Lett. 97 (21) (2006) 216803.
[14] K. Wakabayashi, et al., Electronic and magnetic properties of nanographite ribbons, Phys. Rev. Lett. 59 (12) (1999) 8271–8282.
[15] L. Yang, et al., Quasiparticle Energies and band gaps in graphene nanoribbons, Phys. Rev. Lett. 99 (18) (2007) 186801.
[16] Y. Miyamoto, K. Nakada, M. Fujita, First-principles study of edge states of H-terminated graphitic ribbons, Phys. Rev. Lett. 59 (15) (1999) 9858–9861.
[17] Y.-W. Son, M.L. Cohen, S.G. Louie, Half-metallic graphene nanoribbons, Nature 444 (7117) (2006) 347–349.
[18] N.V. Krainyukova, E.N. Zubarev, Carbon honeycomb high Capacity Storage for Gaseous and Liquid Species, Phys. Rev. Lett. 116 (5) (2016) 055501.
[19] Z. Pang, et al., Bottom-up Design of three-dimensional carbon-honeycomb with Superb Specific strength and high thermal conductivity, Nano Lett. 17 (1) (2017) 179–185.
[20] X. Gu, et al., On the influence of junction structures on the mechanical and thermal properties of carbon honeycombs, Carbon 119 (2017) 278–286.
[21] G. Kresse, J. Furthmüller, Efficiency of ab-initio total energy calculations for metals and semiconductors using a plane-wave basis set, Comput. Mater. Sci. 6 (1) (1996) 15–50.
[22] G. Kresse, J. Furthmüller, Efficient iterative schemes for ab initio total-energy calculations using a plane-wave basis set, Phys. Rev. Lett. 54 (16) (1996) 11169.
[23] P.E. Blöchl, Projector augmented-wave method, Phys. Rev. Lett. 50 (24) (1994) 17953.
[24] J.P. Perdew, K. Burke, M. Ernzerhof, Generalized gradient approximation made Simple, Phys. Rev. Lett. 77 (18) (1996) 3865–3868.
[25] A. Togo, I. Tanaka, First principles phonon calculations in materials science, Scripta Mater. 108 (2015) 1–5.
[26] S. Reich, et al., Tight-binding description of graphene, Phys. Rev. Lett. 66 (3) (2002) 035412.
[27] J. Friedel, in: Dislocations: International Series of Monographs on Solid State Physics, vol. 3, Elsevier, 2013.
[28] J. Liu, et al., A new metallic carbon allotrope with high stability and potential for lithium ion battery anode material, Nano Energy 38 (2017) 263–270.
[29] R. Saito, et al., Electronic structure of graphene tubules based on C60, Phys. Rev. Lett. 46 (3) (1992) 1804–1811.
[30] N. Park, J. Ihm, Electronic structure and mechanical stability of the graphitic honeycomb lattice, Phys. Rev. Lett. 62 (11) (2000) 7614–7618.
[31] R. Saito, et al., Electronic structure of chiral graphene tubules, Appl. Phys. Lett. 60 (18) (1992) 2204–2206.
[32] W. Li, et al., Experimental realization of honeycomb borophene, Sci. Bull. 63 (5) (2018) 282–286.
[33] Y. Wei, R. Yang, Nanomechanics of graphene, Natl. Sci. Rev. (2018), https://doi.org/10.1093/nsr/nwy067.